Porometric Properties of Siliciclastic Marine Sand: A Comparison of Traditional Laboratory Measurements With Image Analysis and Effective Medium Modeling

Allen H. Reed, Kevin B. Briggs, and Dawn L. Lavoie

***Abstract*—During the 1999 sediment acoustics experiment (SAX99), porometric properties were measured and predicted for a well sorted, medium sand using standard laboratory geotechnical methods and image analysis of resin-impregnated sediments. Sediment porosity measured by laboratory water-weight-loss methods (0.372 $\pm$ 0.0073 for mean $\pm$1 standard deviation) is 0.026 lower than determined by microscopic image analysis of resin-impregnated sediments (0.398 $\pm$ 0.029). Values of intrinsic permeability (m^2) determined from constant-head permeameter measurements ($3.29 \times 10^{-11} \pm 0.60 \times 10^{-11}$) and by microscopic image analysis coupled with effective medium theory modeling ($2.78 \times 10^{-11} \pm 1.01 \times 10^{-11}$) are nearly identical within measurement error. The mean value of tortuosity factor measured from images is 1.49 $\pm$ 0.09, which is in agreement with tortuosity factor determined from electrical resistivity measurements. Slight heterogeneity and anisotropy are apparent in the top three centimeters of sediment as determined by image-based porometric property measurements. However, the overall similarity for both measured and predicted values of porosity and permeability among and within SAX99 sites indicates sediments are primarily homogeneous and isotropic and pore size distributions are fairly uniform. The results indicate that an effective medium theory technique and two-dimensional image analysis accurately predicts bulk permeability in resin-impregnated sands.**

***Index Terms*—Permeability, porometry, porosity, porous media.**

I. Introduction

SEDIMENT pore space geometry is often characterized by three porometric properties: porosity, permeability, and tortuosity factor (*sensu* sinuosity) [1]–[4]. These porometric properties exert significant influence on fluid motion in sediments and therefore play a major role in determining acoustic propagation in poro-elastic media, such as marine sands [1]–[4]. To evaluate the significance of these and other seafloor properties to acoustic scattering, penetration, and propagation modeling, the sediment acoustics experiment (SAX99) was conducted in a relatively uniform sandy sediment off the Florida Panhandle near Fort Walton Beach [4]–[6]. Porometric property measurements were made using traditional geotechnical [7], electrical resistivity [8], [9], and image analysis methods [10]–[13]. The primary objectives of this paper are to quantify and compare values of porosity, permeability, and tortuosity factor at decimeter to millimeter length scales using traditional geotechnical and image analysis techniques; to assess and compare spatial homogeneity and isotropy within and among individual sites; and to evaluate the accuracy of image-based porometric characterization and modeling.

This paper discusses the nature of porometric properties and ranges of values for these properties in sand; the validity of using two-dimensional (2-D) image analysis to predict three-dimensional (3-D) properties; and the use of an effective medium technique to make accurate, high-resolution (centimeter-scale) predictions of permeability from 2-D images of resin-impregnated marine sand.

II. Porometric Properties

Porometric properties (i.e., porosity, permeability, and tortuosity factor) were determined by traditional geotechnical methods, image analysis measurements [10], [13] and image analysis/effective medium theory modeling [11], [12] for water-saturated sand. Porosity (n) is the proportion of water volume to the total bulk volume of fully water- saturated sediment and was determined by water-weight loss of dried samples and by pixel-counting of segmented (thresholded) scanning electron microscopy (SEM) images of resin-impregnated sediments. Fluid flow through sediments can be related to hydraulic conductivity or Darcy's coefficient of permeability (K)

$$K = k\frac{\rho g}{\mu}. \tag{1}$$

Darcy's coefficient of permeability in fully saturated sediment is controlled by fluid viscosity (μ), fluid density (ρ), gravitational acceleration (g), and the intrinsic permeability (k), which accounts for the geometrical complexity of pore channels. Values of k are often, as in this study, determined from measured hydraulic conductivity and tabulated values of fluid dynamic viscosity, fluid density, and gravitational acceleration. Hydraulic conductivity is an important component in the volumetric flow equation of Darcy's Law

$$Q = KA\frac{\Delta h}{l}. \tag{2}$$

This equation describes the volumetric flow rate (Q) mediated by the difference in hydraulic "head" (Δh) through a sediment-filled tube of cross-sectional area A and length l. For Darcy's

Manuscript received November 19, 2001; revised July 3, 2002. This work was supported in part by the Office of Naval Research (J. Simmen—Program Manager) and in part by the Naval Research Laboratory Program Element 0601153N under contribution JA/7430-01-0013.

A. H. Reed and K. B. Briggs are with the Seafloor Sciences Branch, Naval Research Laboratory, Stennis Space Center, MS 39529-5004 USA.

D. L. Lavoie is with the Department of Coastal and Marine Geology, United States Geological Survey (USGS), Arlington, VA 22217-5660 USA.

Publisher Item Identifier S 0364-9059(02)06421-X.

Law to be valid, the flow must be laminar, "creeping" flow (see [14] or [15, p. 160]) where viscous forces dominate inertial forces, such that the Reynolds number is very low ($<$10) [15], (see [16, pp. 143–144]). For isotropic media where the fluid flow is aligned with the pressure gradient, Darcy's Law can be equated with the Hagen–Poiseuille equation

$$Q = \frac{\pi r^4}{8\mu}\frac{\Delta P}{l} \tag{3}$$

which applies to isolated, nonconnected, single-sized circular tubes and indicates the relative importance of the tube radius (r). In (3), ΔP denotes the pressure difference between the ends of the tube of length l. By equating Darcy's Law to the Hagen–Poiseuille equation, intrinsic permeability can then be determined as

$$k = \frac{\pi r^4}{8A} \tag{4}$$

which works well to predict intrinsic permeability for a single, straight, uniform tube, but it fails to account for the complexity of natural sediments, which contain multi-dimensioned and interconnected pores. The deviations in these paths require the fluid to travel a distance farther than the shortest distance across the sample. This deviation can be expressed as the tortuosity factor defined by $\langle (L_S/L)^2 \rangle$ [17]–[20], where L_S is the minimum length of a fluid flow streamline between the start and end points of the flow path and L is the length of a straight line between the start and end points of that flow path. In practice L_S, is calculated from a line through the medial axis of the shortest fluid flow path. The tortuosity factor is defined by the average of $(L_S/L)^2$ over the set of all start and end points in the sample, but as discussed later, the separation of the start and end points of the path must be greater than a minimum value. The tortuosity factor thus determined is analogous for hydraulic and electrical systems [21] in siliciclastic marine sand, which has fully interconnected pore space [22] as with SAX99 sediments.

Typical measured values for porosity, permeability, and tortuosity of sand-sized naturally occurring porous media fall within the ranges determined for minimum and maximum density conditions (a function of packing) of idealized sand comprised of mono-sized, spherical beads. For this ideal system porosity may range from 0.27 to 0.48 (see [16, p. 86]), intrinsic permeability between 10^{-13} and 10^{-10} m^2 (hydraulic conductivity between 10^{-6} and 10^{-3} m·s^{-1}) (see [16, p. 98] and [19, p. 136]), and tortuosity factor between 1.3 and 2.2 [19], [20]. In "clean" (i.e., $<$5% particles smaller than 62 μm) sands the values of these porometric properties are also influenced by grain shape, sorting, and size distribution [23], [24]. Despite the morphological and statistical variations within naturally occurring sands, values of porometric properties often fall within much narrower subsets of these ranges, which may reflect that naturally occurring marine sands are often packed to near maximum density. Medium-sized, well-sorted marine sands tend to have average porosity values near 0.38 [16], intrinsic permeability values about 10^{-11} m^2 or hydraulic conductivity values about 10^{-4} m·s^{-1} [16], and tortuosity factors of about 1.5 (see [18, pp. 45–46]). The validity of these representative values of porometric properties for the sandy sediments at SAX99 experiments will be determined by measuring the porometric properties directly and by predicting the properties with 2-D image analysis techniques.

III. Porometric Property Predictions From 2-D Images

Predicting 3-D porometric properties from 2-D data has been addressed by many researchers for sandstone [10]–[13], [25]–[27]. Two basic underlying assumptions in these studies are that the structure of the sandstone is homogeneous and isotropic and that the 2-D images cover an area large enough that microscopic variability (see [19, p. 20]) does not dominate the predictions. To obtain reliable results, the image size should be larger than the "representative elemental area." For areas larger than the representative elemental area, average properties are independent of the area (i.e., the property of "self-similarity" applies) and reflect the values for the bulk volume. For sands from an area similar to the SAX99 site, porosity was shown to be invariable over length scales of four to eleven grain diameters [28]. A length of four-grain diameters is similar to the predicted length scale required for porosity to obtain a stable, asymptotic value [29] and is the same minimum length scale for porosity determined for glass beads [30]. The image size required to reach a stable, asymptotic value, however, may not be the same for porosity, permeability, and tortuosity factor. Based upon the minimum length scales reported above for porosity [28], [30] the image size of 3.5 mm $\times$ 3.5 mm ($\sim$8 grain diameters) was selected for this study. Thirty images for porosity and permeability and five images for tortuosity factor were used for each site. Porometric model accuracy, whether a representative elemental area is established or not, is determined by how well model predictions based on image analysis agree with measurements made by traditional geotechnical techniques. Previous researchers have demonstrated that the characterization of the volumetric pore space represented in 2-D images of a homogeneous and isotropic sandstone are adequate to predict values of porometric properties [10]. Pixel counting, network modeling, and "shortest" path (i.e., streamline) algorithms are often used to predict these properties. Porosity determined from 2-D images as the ratio of void space pixels to the total area [12], [13] usually predicts bulk porosity (e.g., water-weight loss or helium porosimetry) to within a few percent provided the image contains a representative elemental area and the sediment is not heterogeneous. The accuracy of porosity values derived from 2-D images is largely controlled by the image resolution and the segmentation algorithm used to separate the image into void and grain space [31]. Segmentation can be compromised by operator bias due to different selections in the segmentation (thresholding) number [13]. Errors associated with segmentation are discussed in Section VI-B.

A variety of approaches have been used to successfully predict permeability from 2-D images, with emphasis on combining pore geometry quantified in 2-D images with well established laws of fluid flow. For example, intrinsic permeability was predicted to within a factor of 2 for the Benoist sandstone using image analysis techniques [32], [33] to quantify pore sizes, which were incorporated into a modified "bundle-of-tubes" model. Permeability was also accurately predicted for glass beads and a homogeneous sandstone (Berea) using a modified, semi-empirical Kozeny–Carman equation, which established permeability as a function of image porosity, specific surface area, and measured formation factor [27]. Permeability for Brent sandstone was predicted to within a factor of 3 using 3-D reconstructions based upon 2-D correlation functions, a simulated annealing method, and Stokes Law [29]. In all these cases direct permeability predictions from 2-D image data required empirically or implicitly determined components, because 2-D pore geometry (e.g., pore connectivity, formation factor, and specific surface area) does not fully reflect the 3-D geometry.

As noted previously, the tortuosity factor in sediments is defined as the average of the squared ratio of shortest path along fluid flow streamlines to a "straight line" between the start and end points of that path [19, p. 111]. Ideally, the average would be taken over the set of all end points in the sample with a separation at least as large as the side length of the representative elemental area. In practice, the tortuosity factor is obtained by averaging over only the paths that extend the full width of the 2-D image (or length of the sample) [18]–[20]. Tortuosity factor has been determined to vary widely depending upon the analytical method used. Specifically, tortuosity factor determined by diffusion calculations for sand-sized porous media has been reported to be as high as 6.1 [34], whereas it has typically been assumed to be 1.5 based upon the concept that flow paths deviate by ~45° from the direction of the pressure gradient [18]. Image analysis provides, perhaps, the most direct method to determine the geometry of the flow paths and thereby enables direct calculations of the tortuosity factor.

IV. Effective Medium Theory for Permeability Prediction

An effective medium technique (EMT), which accounts for the multidimensional and converging/diverging nature of the pore network (i.e., pore sizes are not uniform nor uniformly distributed), was used to predict permeability in SAX99 sands. The aim of EMT is to infer an average conducting parameter for heterogeneous disordered media from the statistics of local conducting elements [35]. This technique was initially developed to study random resistor networks [36], which are good analogies of pore networks in sedimentary rocks [37], [38]. Doyen [12] demonstrated that sufficient information about the pore structure is available from 2-D images to allow EMT to predict permeability of Fontainebleau sandstones to within a factor of two. His approach was therefore adopted to predict permeability from high-resolution images of SAX99 sands. An abbreviated version of the EMT used in [12] and adopted for this study is described below. The reader is referred to [11], [12] or [35] for additional details.

EMT assumes the bulk hydraulic conductivity is determined by the geometry and interconnectedness of the pore space, because the rock frame (or sediment grains in this case) is a nonconducting material. The hydraulic conductivity of the system is related to total porosity, and the statistical distributions of pore body size (i.e., the "nodes" or wider parts of the pore space), cross-sectional area of pore throats (i.e., "bonds" or constrictions that join pore bodies), coordination number (i.e., the number of pore throats that connect to the pore bodies), and tortuosity factor. The pore network is considered an interconnected and randomly directed grouping of "tubes" and, in keeping with the Hagen–Poiseuille Law (2), the cross-sectional area of the pore throats (or "tubes") is the primary geometrical determinant of the fluid flow.

EMT assumes sediments contain a heterogeneous, noncorrelated distribution of pore throats. The goal is to replace the distribution of pore throats by a single effective pore throat radius r^*, and the challenge is to determine r^* such that the total fluid flow through the pore network is unchanged for a given external pressure difference. In doing this, it is convenient to introduce the hydraulic conductance $g(r)$ [11] for a cylindrical pore throat of radius r defined by

$$g(r) = \mu Q/\Delta P. \tag{5}$$

In (5), the volumetric flow rate Q depends on the throat radius, but that is not indicated explicitly. From (3), the hydraulic conductance for a straight, cylindrical pore throat of radius r and length l is given by

$$g(r) = \frac{\pi r^4}{8l}. \tag{6}$$

In this equation, l is assumed to be a constant proportional to the mean grain diameter, which may overestimate the actual length of the pore throats in the case of maximum density packing.

We assume the probability distribution function of pore throat radii $n_t(r_i)$ has been determined in the form of a histogram, where r_i denotes the ith radius interval, and where $n_t(r_i)$ denotes the probability that the pore radius is within the ith interval. Then the effective pore throat radius r^* for EMT is given by the following equation [36]:

$$\sum_i n_t(r_i)\frac{g(r^*) - g(r_i)}{g(r_i) + [(z/2) - 1]g(r^*)} = 0 \tag{7}$$

which is solved iteratively to obtain r^*. In (7), z is the average coordination number for all the pore bodies, which exerts a small influence in this calculation because conductivity values increase very gradually with increasing coordination numbers [14]. The coordination number for each pore body is determined by counting the number of throats that intersect at the pore body.

Once r^* has been determined by self-consistency from (7), it is possible to solve for the permeability using (4) by replacing r by r^* and A by the area $\pi \cdot \langle r_{pc}^2 \rangle$ representing the average pore space over which the conduction is occurring, where $\langle r_{pc}^2 \rangle$ is the spatial average of the square of the pore channel radius. When modeling permeability in natural sediments, it is also necessary to take into the account the porosity (n) of the system and the deviation in the path length and path direction using the tortuosity factor (T). These parameters determined from 2-D images can be incorporated into (4), leading to the following expression for permeability [12]:

$$k = \frac{n}{8T}\,\frac{r^{*4}}{\langle r_{pc}^2 \rangle}. \tag{8}$$

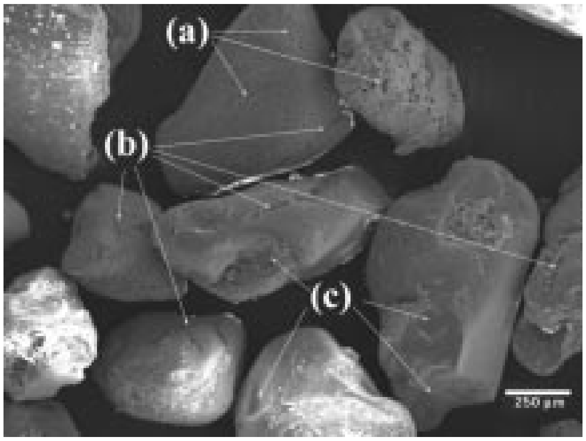

Fig. 1. Scanning electron microscope images of sand grains, collected from the SAX99 experimental site offshore Fort Walton Beach, FL. Typical features of siliciclastic marine sands include: (a) grooves or pits; (b) linear fractures; (c) conchoidal fractures.

A tortuosity value of 1.5 was used in (7) for all permeability predictions, because this was the measured average from several images (Table II) from two locations at the SAX99 site (the "Lopes" site and the "ARL-UT" site).

V. Geologic Setting and Sediment Characteristics

The West Florida Sand Sheet [39] is a homogeneous surficial body of relict quartz sands [40] located on the continental shelf offshore from Panama City, FL, and extending west to across the Alabama state line. These sands, primarily derived from the Appalachian Mountain system, were transported through the Apalachicola fluvial and estuarine systems during the Plio–Pleistocene period and were delivered to the present location by nearshore currents. Currently the sand deposits at the SAX99 experimental site are part of a shoreface-connected sand ridge that is in equilibrium with hydrodynamic conditions [6]. The result is a homogeneous sand deposit of relict quartz sand, with small percentages of recently introduced carbonate (e.g., shells) and clay sediment [6], [40], [41].

Individual grains display features typical of marine quartz sands [42], such as linear and conchoidal fractures, pits, and grooves (Fig. 1). The surface morphology and grain shape is much more complex than that of spheres or plates and plays a fundamental role in determining grain–grain interactions, pore sizes and distribution, sediment porosity, permeability, tortuosity, formation factor, bulk density, and frame rigidity.

VI. Sample Collection and Analyses

A. Diver Core Collection and Analysis

Scuba divers carefully collected sediment samples in 6.1-cm diameter (5.9-cm ID), clear, polycarbonate core tubes by hand for porometric analysis by traditional geotechnical methods [6], [8], image analysis [12], [13] and image analysis/effective medium theory modeling [11], [12]. Cores were handled carefully and maintained in a vertical position until porosity and permeability analyses or resin impregnation was performed. Cores were discarded if sediment disturbance was noted. Samples were collected near the site of five SAX99 acoustic measurement experiments [5]: Benthic Acoustic Measurement System (BAMS), Sediment Transmission Measurement System (STMS), Coastal Systems Station (Lopes), low frequency (LF), and Applied Research Lab-University of Texas (ARL-UT) (Table I). Percent water content was determined gravimetrically by measuring the water-weight loss after drying at 105 °C for 24 h from 2-cm interval subsamples of undisturbed diver-collected cores. Because water content measurements required use of an analytical balance, these cores were isolated from vibration and carefully transported to the shore-based laboratory prior to analysis. Measured values of average grain density were used to calculate porosity from water content [43]. Porosity values were corrected for salt content. The sediment grain size distribution was measured from disaggregated samples by dry sieving with a sieve shaker for gravel- and sand-sized particles. In addition, pipettes were used for silt- and clay-sized particles (never more than 5% of total weight) and the distribution was expressed as a weight percentage [43]. Mean grain size (mm) was estimated by the graphic method of Folk [44]. Phi size (ϕ) is equivalent to the negative base-two logarithm of the diameter expressed in millimeters.

TABLE I
Coordinates of the SAX99 Sites for Which Data is Presented

Site	Latitude (N)	Longitude (W)
STMS	30° 22.671′	86° 38.695′
ARL-UT	30° 22.648′	86° 38.695′
Lopes	30° 22.578′	86° 38.657′
LF	30° 22.806′	86° 38.700′
BAMS	30° 22.680′	86° 38.802′

Hydraulic conductivity was measured by a constant-head permeameter technique on whole cores while aboard ship [6] within one day of core collection. For this experiment, 13-cm-long cores (6.1-cm diameter) were collected such that the sediment completely filled the core liner from top to bottom. Hydraulic conductivity (K) was determined with a Soiltest K-605 combination permeameter, which was modified to accommodate the entire 13-cm-long core [45]. For each core, five consecutive measurements were made as surface seawater percolated through the core as a result of the constant hydraulic head. The intrinsic permeability (k) of the sediments is then found from (1). The fluid density and dynamic viscosity needed in (1) were calculated from temperature and salinity of surface seawater from the SAX99 site [6] at the time the measurement was made.

B. Image Analysis and Predictions From Pore Geometry

High-resolution image analyses were performed on resin-impregnated sediments. Sediments in two cores were impregnated aboard the ship within 24 h of collection using a polyester casting resin, which solidified prior to transport to the shore-based laboratory [6]. Considerations made for choosing a suitable resin depend on the grain and pore sizes, resin viscosity [46], and degree of water saturation. A resin was used that could be applied in water-saturated samples for medium-sized sand and could be prepared to a fairly low viscosity. Multicomponent polyester casting resins have worked well for binding water-saturated sands *in situ* [47]–[49] and are ideal for

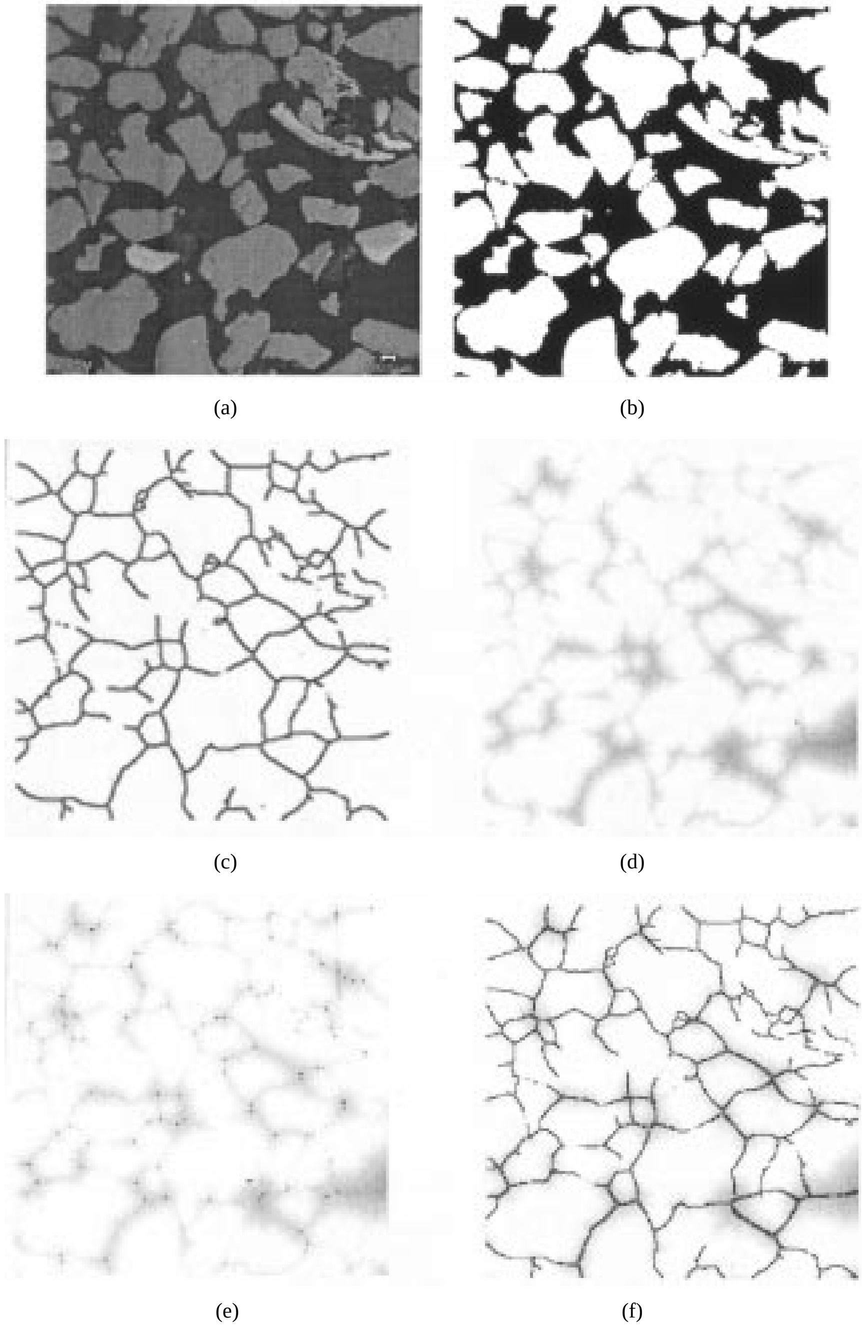

Fig. 2. Scanning electron image (SEM) of a section cut from a resin-embedded core is used to determine pore geometry by converting (a) the SEM image into (b) a binary image from which (c) a medial axis (skeleton) and (d) a Euclidean Distance Map (EDM) (burn image) are created. (e) Pore body/EDM and (f) pore throat/EDM images enable the quantification of the pore body and pore throat sizes. Coordination number is determined from (c). Scale bar in (a) is 100 μm and all images are 3.5 mm $\times$ 3.5 mm. The binary image (b) depicts plucked grains (gray), pore space (black), and grains (white). The gray areas are painted white prior to the image analysis.

marine sands because they: 1) attain low viscosity by mixing and without heating; 2) cure without heating; and 3) maintain constant volume during curing. To detect possible sediment volume changes during the resin-impregnation process, the sediment water interface was marked on the outside of the cores, with a 1-mm-wide line, after cores were returned to the ship and prior to resin impregnation. No changes in the position of the sediment water interface were noted after the resin cured; therefore, the volumetric change in sediments due to resin impregnation was at most $\pm$0.05%. Once cured, two, 1-cm-square blocks were cut from each 1-cm depth interval. The blocks were polished smooth and surfaces parallel and horizontal to the sediment water interface were digitally imaged with either a Hitachi S3500 Environmental Scanning Electron Microscope (ESEM) or an Amray 1820 Scanning Electron Microscope (SEM) in backscatter electron mode. The "parallel" block surface images are from the top 1.0 mm of the indicated depth intervals, whereas the "perpendicular" block images are from mid-depth of the interval. Image resolution (i.e., pixel size) is 6.9 μm.

Digital SEM images of 3.5 mm $\times$ 3.5 mm areas from the polished blocks [Fig. 2(a)] were converted to binary images (a

1-bit bitmap) [Fig. 2(b)] to determine pore and grain geometry using Adobe Photoshop 5.5 equipped with the Image Processing Toolkit 3.0 [50]. Pore sizes were quantified using a calibrated length scale in Uthsca Image Tool 2.0 [51]. To ensure measurements overcame the microscopic effects of small sample size, an image length of about 8-grain diameters was used (cf. the minimum length to predict bulk porosity is approximately equal to 4 grain diameters for homogeneous sand and glass beads [30]). This area provides the highest possible resolution for porosity, permeability and tortuosity factor while maintaining a representative elemental area for "clean" sands.

Pore geometry was evaluated by converting the digital SEM image [Fig. 2(a)] into a binary image [Fig. 2(b)], in which pore pixels are black and grain pixels are white using a simple segmentation technique. Porosity (n) was determined by pixel counting, where porosity is equal to the sum of pore pixels in the image divided by the total number of pixels in the image.

Segmenting images into the grain and pore phases can lead to inaccuracies for two reasons. First, the segmentation process employs a simple thresholding technique to achieve the best fit to the image, which is always selected by "eye." This process allows the processor to account for variable image quality that often results from fluctuating beam intensities that occur over several hours to days of image collection. Second, some grains, especially the highly fractured ones, are invariably plucked out of the resin during the polishing process. The depressions in the resin from which the grains were plucked are "painted" white using Adobe Photoshop 5.5. To ensure that the segmented images maintained the grain–pore boundaries a simple self-consistency test was employed using Adobe Photoshop 5.5. The opacity of the segmented image was increased, while ensuring that the pore and grain shapes were still clearly visible. These images with enhanced opacity were compared to the original SEM images to ensure that the grain–pore boundaries were unchanged to within a pixel.

These binary images are then duplicated so that the medial axis (skeleton) image [Fig. 2(c)] and a Euclidean Distance Map (EDM) [Fig. 2(d)] are made from the original binary image. The medial axis [Fig 2(c)] traces the central (median) path of the pore network, enables the quantification of the coordination number and displays the interconnectivity of the pore network. The medial axis image [Fig. 2(c)] is then segmented to obtain a pore body (i.e., the junction for pore throats) image (not shown) and a pore throats (i.e., the bonds that connect the pore bodies) image (not shown). These images are laid on top of EDM images to produce pore body/EDM [Fig. 2(e)] and pore throat/EDM [Fig. 2(f)] images. Pore body radii are determined from the pore body/EDM image and pore throat radii and lengths are determined from the pore throat/EDM image. These measured pore parameters are used to determine intrinsic permeability (k) using (7). An important consideration in these measurements is the associated error, which is directly proportional to the resolution of the images. Each measurement is considered accurate to within ± 1 pixel length (~ 6.9 micrometers for a 512-$\times$-512-pixel image). In the intrinsic permeability predictions this error translates to maximum errors of a factor of 2 above or below the calculated permeability values. Hydraulic conductivity (K) was calculated using (1) from modeled values of intrinsic permeability (k) derived from image analysis and values of fluid dynamic viscosity and density determined from temperature and salinity of seawater from the SAX99 site.

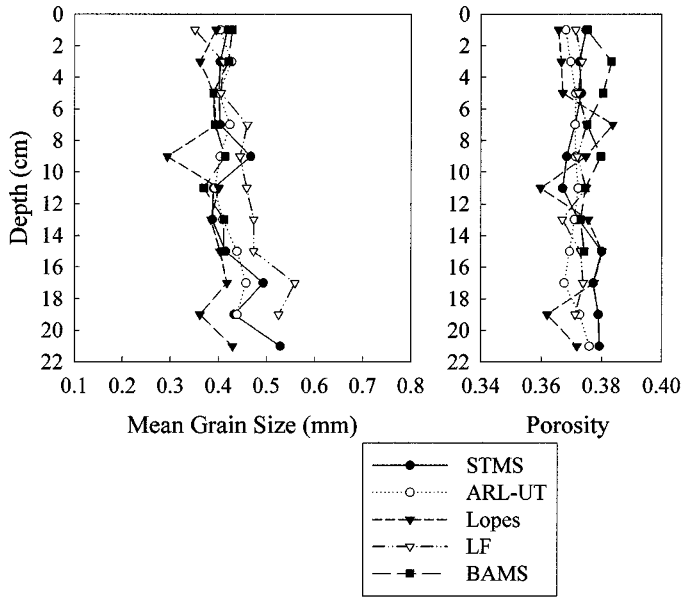

Fig. 3. Vertical distribution of sediment porosity (from water-weight-loss method) and mean grain size at SAX99 indicate slight amounts of variability.

TABLE II
AVERAGE POROSITY, PERMEABILITY, AND TORTUOSITY FACTOR MEASUREMENTS MADE ON SEDIMENTS FROM THE SAX99 SITES

Direct Measurements					
Site	Porosity (n)	$\pm\sigma$	Permeability (10^{-11} m^2)	$\pm\sigma$ (10^{-11} m^2)	
STMS [a]	0.373	0.008	3.29	0.33	No tortuosity factor measurements were made
ARL-UT [b]	0.371	0.006	2.93	0.83	
Lopes [c]	0.371	0.008	3.69	0.28	
LF [d]	0.372	0.007	3.83	0.03	
BAMS [d]	0.377	0.007	3.07	0.05	
Image Analysis Determinations					
	Porosity (n)	$\pm\sigma$	Permeability (10^{-11} m^2)	$\pm\sigma$ (10^{-11} m^2)	Tortuosity factor $\langle (L_s/L)^2 \rangle$
ARL-UT (hor.) [e]	0.393	0.024	2.91	1.13	1.54
(vert.) [e]	0.399	0.018	2.85	1.10	1.45
Lopes (hor.) [e]	0.394	0.017	2.79	0.49	1.45
(vert.) [e]	0.405	0.019	2.57	0.97	1.51

[a] 5 cores for porosity and 3 cores for permeability, [b] 8 cores for porosity and 4 cores for permeability, [c] 1 core for porosity and 2 cores for permeability, [d] 2 cores for porosity and 2 cores for permeability, [e] 30 images for each porosity and permeability measurement and five images for each tortuosity measurement

VII. RESULTS

A. Traditional Measurements

SAX99 sediment is well sorted, medium sand ranging from a mean diameter of 0.29 to 0.56 mm [Fig. 3(a)]. Sediment shape based on the Power's roundness scale [52] is sub-rounded to sub-angular. Sediment porosity, adjusted for porewater salinity, averaged 0.372 $\pm$ 0.0073 ($\pm\sigma$) for all SAX99 sites (Table II) and displayed only slight variability [Fig. 3(b)]. In every case that follows, the mean values are given $\pm$one standard deviation (σ). Hydraulic conductivity measured in the upper 13 cm from cores collected at the ARL-UT, BAMS, STMS, LF, and Lopes locations at the SAX99 site averaged $3.6 \times 10^{-4} \pm 0.7 \times 10^{-4}$

TABLE III
VALUES FROM CORES OF HYDRAULIC CONDUCTIVITY (K), INTRINSIC PERMEABILITY (k), AND MEAN GRAIN SIZE FOR FIVE LOCATIONS AND FOUR SEDIMENT DEPTHS AT THE SAX99 SITE

Location	Sediment Depth (cm)	K (10^{-4} m s^{-1})	k† (10^{-11} m^2)	Mean Grain Size (phi)	Mean Grain Size (mm)
Lopes	0-13	3.9	3.4	1.43	0.37
Lopes	0-13	4.4	4.0	1.43	0.37
BAMS	0-13	3.3	3.1	1.32	0.40
BAMS	0-13	3.2	3.0	1.32	0.40
LF	0-13	4.2	3.8	1.22	0.43
LF	0-13	4.2	3.8	1.22	0.43
ARL-UT	0-13	3.9	3.6	1.29	0.41
ARL-UT	0-13	2.9	2.7	1.29	0.41
ARL-UT	0-13	4.0	3.7	1.29	0.41
ARL-UT	0-13	1.8	1.7	1.29	0.41
STMS	0-13	3.9	3.7	1.29	0.41
STMS	0-13	3.0	2.9	1.29	0.41
STMS	0-13	3.4	3.3	1.29	0.41
Average	**0-13**	**3.6**	**3.3**	**1.32**	**0.40**
STMS	20-33	5.1	5.1	1.09	0.47
STMS	34-45	4.8	4.7	1.02	0.49
STMS	43-55	4.0	4.0	1.14	0.45

†The conversion from K to k is not a constant proportion, because the calculation of k from (1) is dependent upon dynamic viscosity and fluid density, which change with varying temperature of surface seawater.

m·s^{-1}, which corresponds to an intrinsic permeability of 3.3 $\times$ 10^{-11} $\pm$ 0.60 $\times$ 10^{-11} m^2 (Table III). At the STMS site permeability values measured at depths below 13 cm are slightly higher, likely due to an increase in the number of shell particles in those depth intervals.

B. Predictions From Image Analysis

Sediment porosity (from pixel counting) averaged 0.398 $\pm$ 0.029 (range = 0.336 to 0.478) in the top ten centimeters below the sea floor at the Lopes and ARL-UT sites (Table II). Intrinsic permeability at the Lopes and ARL-UT sites averaged 2.78 $\times$ 10^{-11} $\pm$ 1.01 $\times$ 10^{-11} m^2, which when fluid properties of seawater at the SAX99 site are accounted for corresponds to a hydraulic conductivity of 2.93 $\times$ 10^{-4} $\pm$ 0.74 $\times$ 10^{-4} m·s^{-1} (Table II; Fig. 4). Values of permeability in 2 intervals (0–1 and 2–3 cm) at the Lopes site and one interval (0–1 cm) at the ARL-UT site are slightly anisotropic. However standard deviations for all other values of permeability at the Lopes (1–2 and 4–10 cm) and ARL-UT (1–10 cm) sites overlap, indicating that the sediments are fairly isotropic with respect to permeability (Fig. 4). The Lopes site has lower variability in permeability predictions than the ARL-UT site at depths below 5 centimeters. Tortuosity factor averaged 1.49 $\pm$0.09 in the top ten centimeters below the seafloor at the Lopes and ARL-UT sites (Table II) with a range of 1.35 to 1.60 for the 20 images for which tortuosity factor was measured. This is a reasonable tortuosity factor for sands in the SAX99 study site [23] and for sands in general [18], [19]. While a slight amount of variability exists for the vertical and horizontal sections at the Lopes and ARL-UT sites and also between those sites, the sediments appear to be isotropic with respect to tortuosity factor.

The mean value of porosity determined by the water-weight loss technique is significantly lower (Student's t-test for equal variances) than those determined by the image-analysis technique. The mean value of permeability determined by constant head permeameter measurement is also significantly higher than those determined by image analysis and EMT. The implications of these differences are discussed in Section VIII.

One of the principal objectives of the SAX99 experiment was to characterize variability in sedimentary structure and sediment properties [6]. Variability in sediment structure is controlled by variations in grain size, sorting, and packing, which correspond to differences in pore size distribution, and values of tortuosity, porosity, and permeability. Most images depict homogeneous and isotropic sedimentary structure, but some heterogeneity and anisotropy are also present, especially in sediments near the surface. To provide examples of the pore and grain-size variability at discrete depth intervals, several images are depicted in Fig. 5. The porosity values for the homogeneous images [Fig. 5(a) and (b)] are within 0.006, whereas for the heterogeneous images porosity values differ by more than 0.08 [Fig. 5(c) and (d)]. The pore sizes in the interval of isotropic permeability are roughly equivalent, corresponding to permeability values that differ by only 3.0 $\times$ 10^{-13} m^2 [Fig. 5(e) and (f)]. Whereas for the anisotropic sediments, as exemplified by images taken from the 0–1-cm interval of the Lopes site, the average pore sizes are more disparate [Fig. 5(g) and (h)], resulting in a statistically significant difference of 3.26 $\times$ 10^{-11} m^2 in predicted permeability values.

VIII. DISCUSSION

Laboratory measurement of porosity and permeability is considered a routine geotechnical characterization of marine sediments, although issues associated with sample disturbance during sediment collection and transport as well as the loss of water during sectioning cores have lead some authors to question the accuracy of these measurements for sands [9], [53]. Novel and potentially more accurate approaches to measuring these sediment physical properties are therefore needed. Image analysis of resin-impregnated sands, which solidifies the sediment and maintains the pore sizes and spatial grain distributions, is one such novel approach. This image-based technique provides porometric properties over scales much finer than traditional laboratory methods and may provide values of porometric properties more relevant to the spatial scales required for high-frequency acoustic modeling.

Porosity values determined by traditional geotechnical methods have a lower mean, an overall narrower range, and a lower variability than porosity determined by image analysis/pixel counting. The lower values of porosity determined by traditional measurements as compared to image analysis measurements have been noted in other studies [12], [27] and are likely the result of differences in the techniques, but a difference simply due to the natural variability of the sediment cannot be completely ruled out. However, the similarity of porosity values among the five sites where traditional water-weight-loss measurements were made (Table II) suggests that natural variability is not the cause. Issues associated with segmentation effects (i.e., overestimating or underestimating the grain areas) or the discrepancy between 2-D image porosity and 3-D image porosity are unresolved. Greater variability in the estimates of porosity based on image analysis compared to traditional measurements probably exists due to differences in measurement scale between these two techniques. Small-scale

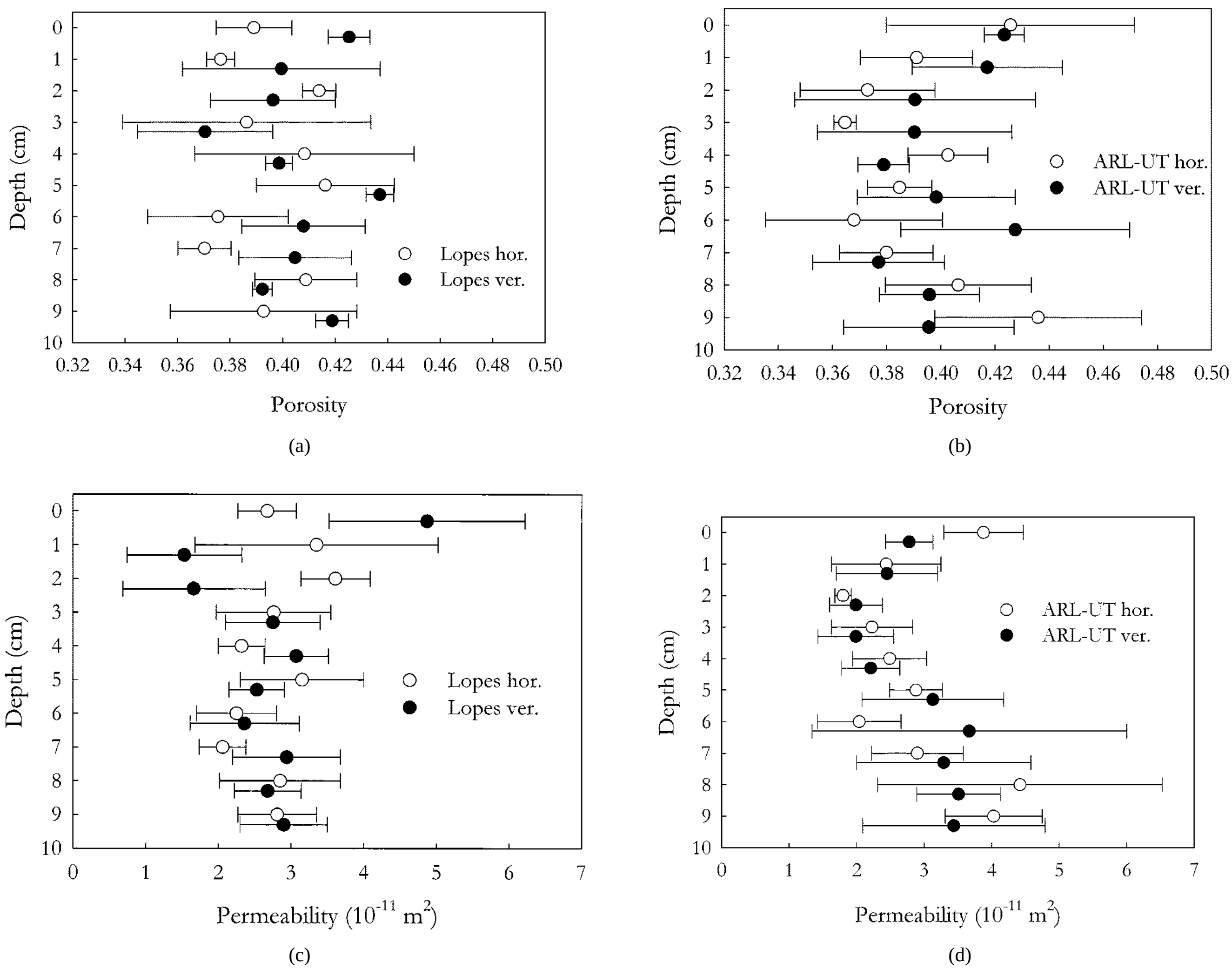

Fig. 4. Porosity determinations at the (a) Lopes; (b) ARL-UT sites. Permeability predictions at the (c) Lopes; and (d) ARL-UT sites from resin-impregnated core sections.

heterogeneity (i.e., differences in grain sizes and total pore volume) that is evident in 12.25-mm^2 area images probably is not resolved from the much larger (28 cm^3) volumes used for water-weight-loss techniques.

There has been considerable speculation on the reason for differences in porosity measured by traditional and image analysis methods in sandstone [12], [13], [27], [28], [33], which includes problems associated with segmentation, a failure to realize a representative elemental area, and sample heterogeneity. These issues also apply to unconsolidated sands found in SAX99 in addition to the effects of sample disturbance. The potential problems associated with segmentation can be evaluated by comparison of grain boundaries before and after segmentation. As discussed previously in Section VI-B, the segmentation of the SEM image is accurate to within a pixel, which translates to a maximum error of ± 0.02. Also as discussed previously, images of SAX99 sands contain at least 8-grain diameters, which should be sufficient to achieve a representative elemental area for a homogeneous sand sample. However, the greater variability of imaged-based porosity compared to water-weight-loss porosity suggests that considerable small-scale variability exists (based upon evaluation of 120 images) at millimeter scales and an individual image is insufficient to reliably determine mean bulk porosity at larger scales. The combination of porosity from multiple images (30 horizontal and 30 vertical images per site) reduced the standard deviation to 0.005 and makes the combined image porosity measurement comparable in size to the elements used for the water-weight-loss techniques. We believe that the representative elemental size was achieved for individual images and the variability found in image-based analyzes reflects small-scale variability present in SAX99 sediment at the millimeter scale. It has also been suggested that resin impregnation may somehow disrupt sediment structure or that image analysis may not realize a representative elemental area given that the sediments may be heterogeneous at high resolution (here: 3.5 mm $\times$ 3.5 mm). To ensure that sediment structure and stability were maintained during impregnation, the sediment volume was monitored. Given that the total-core sediment volume did not change (at most 1 mm in length) in any substantial way, we assume that pore volume, pore sizes, and pore size distributions were not changed by the resin-impregnation process. Our

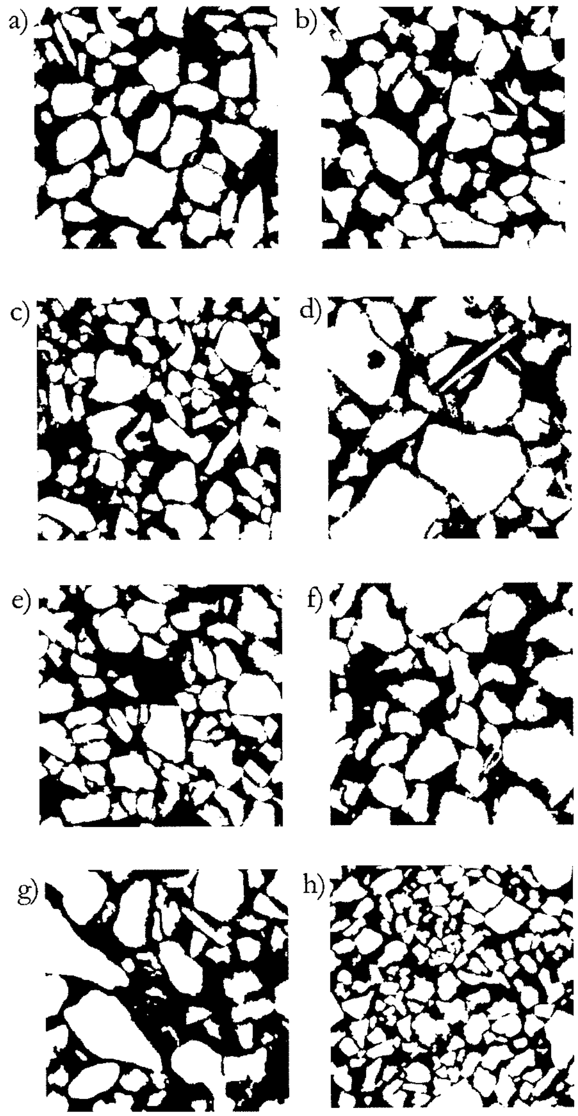

Fig. 5. Representative cases of homogeneity (a), (b), heterogeneity (c), (d), isotropy (e), (f), and anisotropy (g), (h) from vertical and horizontal images provide a conceptual basis for relating grain and pore geometry to porometric properties of the sediments. Homogeneity at ARL-UT 6-7 cm interval is evident from images of (a) vertical ($n = 0.4024$) and (b) horizontal ($n = 0.4019$) sediment sections. Heterogeneity at Lopes 7–8 cm interval is evident from images of (c) vertical ($n = 0.4300$) and (d) horizontal ($n = 0.3481$) sediment sections. Isotropy at Lopes 6–7 cm interval is evident from images of (e) vertical ($k = 2.83 \times 10^{-11}$ m^2) and (f) horizontal ($k = 2.89 \times 10^{-11}$ m^2) sediment sections. Anisotropy at Lopes 0–1 cm interval is evident from images of (g) vertical ($k = 5.79 \times 10^{-11}$ m^2) and (h) horizontal ($k = 2.23 \times 10^{-11}$ m^2) sediment sections. Image size is 3.5 mm × 3.5 mm.

resin-impregnation technique, which uses a direct replacement of water with resin so that the pore spaces are saturated throughout the fluid replacement, maintains pore pressures, and eliminates the increase of intergranular stress that is associated with drying the sediments. This, along with the elimination of multiple alcohol washes ensures that the sediment and pore spaces are subjected to the least amount of alteration.

Traditional geotechnical measurements of porosity are subject to a different sort of criticism. Gravimetric measurements may underestimate porosity due to water loss associated with drainage and evaporation, especially during sectioning or sub-sampling. Comparisons between porosity for subsections and whole cores differ by an average of less than 0.003 [54] suggesting that sectioning, if done carefully, does not result in significant water loss. Both resin-image processing techniques and traditional laboratory techniques may suffer interstitial water loss from disturbance during core collection. This water loss should be greatest in the upper centimeter of sediment where disturbance (e.g., compaction or densification) of loosely packed sediment is probably the greatest [9]. Wheatcroft [9] collected known volumes of sediment from 4–7 cm below the surface during SAX99 experiments in order to provide calibration of resistivity probes. These porosity measurements (0.37 ± 0.02) based on water-weight loss from a known volume of sediment eliminated the effects of sediment disturbance during transport and water-weight loss during laboratory manipulations, but the procedure may still compact sediment during core insertion. These measurements also excluded sediments near the sediment-water interface, which are potentially most susceptible to disturbance [9]. The nearly identical values of porosity measured by the water-weight-loss technique used in this paper and those in [9] lend credence to the water-weight-loss technique.

The degree of sediment packing has a major impact on sediment porosity. Maximum and minimum densities for SAX99 sediments were determined using standard American Society for Testing and Materials (ASTM) [55] laboratory vibratory densification techniques on dried sediments. The maximum density for representative sample of tightly packed SAX99 sand (2071 kg m^{-3}) corresponds to a porosity of 0.368, which is slightly higher than the minimum image porosity of 0.336. The minimum density for loosely packed SAX99 sand (1938 kg m^{-3}) corresponds to a porosity of 0.447, which is lower than the maximum porosity determined by image analysis of 0.478. Relative density (D_r) in percent is defined as

$$D_r = 100\frac{e_{\max} - e}{e_{\max} - e_{\min}} \tag{9}$$

where $e_{\max}$ and $e_{\min}$ are the maximum and minimum values of void ratio measured from the laboratory vibratory densification technique and e is the *in situ* void ratio. The minimum and maximum sediment densities correspond to $e_{\max}$ and $e_{\min}$, respectively. Void ratio is related to porosity by $n = e/(1+e)$. The mean image-based porosity corresponds to a relative density of 65%. Given the range of porosities measured by water-weight-loss techniques (0.356–0.397) relative densities range between 66%–112% with a mean relative density of 94%. If the water-weight-loss measurements are correct or slight underestimates of porosity, *in situ* sediments must be near their maximum density. Underestimates of porosity would be due to compaction during core collection and water loss by drainage or evaporation (e.g., 0.003 to 0.01) during sectioning. The greater range in relative density in image-based porosity compared to water-weight loss is reasonable considering the differences in sample size. Relative density determinations could also be high due to the fact that maximum and minimum void ratios were determined on dry samples. Frazer [56] has demonstrated that porosity values may be 0.005 lower when compacting subaqueously deposited samples. In spite of these problems, this study demonstrates that the mean *in situ* porosity for SAX99 sediments is probably between the values determined by water-weight loss and image processing methods (0.37–0.40). The inability to unambiguously determine a mean porosity value for SAX99 sands by these different methods suggests that further work is needed to resolve the disparities in porosity measurements that result from these and other techniques. We believe differences in these determinations should be seen as a need for future investigations rather than an indictment of either methodology.

Mean permeability determined from traditional geotechnical methods is significantly higher (a difference of 0.51×10^{-11} m^2) than the mean value predicted by image analysis/EMT modeling. While the mean permeability values determined by traditional and image analysis/EMT modeling methods are statistically different, the differences may be within the absolute measurement error of the two techniques and thus may not be physically significant. Errors in image analysis determination of porosity or pore size distribution may over- or underestimate total pore space due to errors in segmentation (thresholding). The error in the porosity value can be bounded by eroding (decreasing) or dilating (increasing) the image pore space by one pixel at the pore-grain boundary and then calculating the image porosity as previously defined for each image. If the errant porosity value obtained by this process ($\pm$0.02) is directly incorporated into (8) the consequent error in permeability is on the order of $\pm 0.125 \times 10^{-11}$ m^2 (or $\pm$5%). If pore spaces were inaccurately segmented to produce pore sizes that are all either too large or too small ($\pm$1 pixel), then permeability predictions would have a maximum error of approximately 100% based on a reduced gradient method. This error is not considered large for sands [25], [27], [33] that potentially have permeability ranges of several orders of magnitude [16].

Tortuosity factor is an important determinant of transport in sediments and accurate determination of this property will aid in the prediction of fluid transport and acoustic propagation. Tortuosity factor measured by image analysis of SAX99 sediments ranged between 1.35 and 1.59 for individual images with a mean of 1.49 ± 0.09. This value of tortuosity factor is similar to the value 1.40 that is obtained from the formation factor (F) determined from resistivity measurements made in [8] using the commonly employed relationship $T = Fn$ [20], which relates tortuosity factor to the formation factor and porosity. Image-based determination of tortuosity factor leads to very similar values compared to the prediction of tortuosity in sands (1.5) [23] in which the deflections in the streamlines are assumed to be about 45° [18] for nearly spherical particles (e.g., glass beads).

IX. Summary and Conclusions

The sediments at the SAX99 site appear homogeneous and isotropic for scales over hundreds of meters to as small as a few millimeters. This large-scale homogeneity (within cores and among sites) reflects the fact that SAX99 experiments were conducted on and the sediments collected from the crest of a single shoreface-connected ridge. Sediments on this ridge are in equilibrium with current hydrodynamic conditions (e.g., waves and currents) [6], which apparently create a uniform surficial deposit. Variability and anisotropy in porometric property measurements measured at the scales of the image analysis, especially in the upper 2 cm of sediment, may be due to small-scale hydrodynamic forcing (e.g., grain fractionation and winnowing) and bioturbation. The large-scale homogeneity generally allows for comparison of acoustic experimental results among different sites within the SAX99 experimental site. However, small-scale variability must be characterized for high-frequency acoustic modeling where spatial volume heterogeneity is important.

The comparison between traditional and image-based values of sediment porosity and permeability demonstrates that image analysis coupled with effective medium theory can provide reasonable estimates of sediment porosity and good estimates of permeability. In addition, the image-based analysis allowed the direct measurement of sediment tortuosity factor, an important input to poroelastic propagation and scattering models. Using these techniques characterization of fine-scale sediment volume heterogeneity was also demonstrated.

Acknowledgment

The authors wish to thank divers M. Richardson, R. Ray, D. Lott, R. McDowell, A. Furet, and J. Phelin for collecting cores during SAX99; J. Watkins for operating the Hitachi S3500 scanning electron microscope; A. Falster for help with and use of the Amray 1820 scanning electron microscope; P. Elmore for help with error analysis; W. Sawyer for running the relative density measurements; E. Thorsos for overseeing the SAX99 experiments; K. K. Mohanty for implementation of EMT; and J. E. Cable, M. Richardson and E. I. Thorsos for critical reviews.

References

[1] M. A. Biot, "Theory of propagation of elastic waves in a fluid saturated porous solid. II. Higher frequency range," *J. Acoust. Soc. Amer.*, vol. 28, no. 2, pp. 179–189, 1956.

[2] ——, "Generalized theory of acoustic propagation in porous dissipative media," *J. Acoust. Soc. Amer.*, vol. 34, pp. 1254–1264, 1962.

[3] R. D. Stoll, "Sediment Acoustics," in *Lecture Notes in Earth Sciences*, S. Bhattacharji, G. M. Friedman, H. J. Neugenbauer, and A. Seilacher, Eds. New York: Springer-Verlag, 1989, vol. 26.

[4] K. L. Williams, D. R. Jackson, E. I. Thorsos, and D. Tang, "Comparison of sound speed and attenuation measured in a sandy sediment to predictions based on the Biot theory of porous media," *IEEE J. Oceanic Eng.*, vol. 27, pp. 413–428, July 2002.

[5] E. I. Thorsos, K. L. Williams, N. P. Chotiros, J. T. Christoff, K. W. Commander, C. F. Greenlaw, D. V. Holliday, D. R. Jackson, J. L. Lopes, D. E. McGhee, M. D. Richardson, J. Piper, and D. Tang, "An overview of SAX99: Acoustic measurements," *IEEE J. Oceanic Eng.*, vol. 26, pp. 4–25, Jan. 2001.

[6] M. D. Richardson, K. B. Briggs, D. L. Bibee, P. A. Jumars, W. B. Sawyer, D. B. Albert, R. H. Bennett, T. K. Berger, M. J. Buckingham, N. P. Chotiros, P. H. Dahl, N. T. Dewitt, P. Fleischer, R. Flood, C. F. Greenlaw, D. V. Holliday, M. H. Hulbert, M. P. Hutnak, P. D. Jackson, J. S. Jaffe, H. P. Johnson, D. L. Lavoie, A. P. Lyons, C. S. Martens, D. E. McGhee, K. D. Moore, T. H. Orsi, J. N. Piper, R. I. Ray, A. H. Reed, R. F. L. Self, J. L. Schmidt, S. G. Schock, F. Simonet, R. D. Stoll, D. Tang, D. E. Thistle, E. I. Thorsos, D. J. Walter, and R. A. Wheatcroft, "An overview of SAX99: Environmental considerations," *IEEE J. Oceanic Eng.*, vol. 26, pp. 26–53, Jan. 2001.

[7] T. W. Lambe, *Soil Testing for Engineers*. New York: Wiley, 1951.
[8] D. Tang, K. B. Briggs, K. L. Williams, D. Jackson, E. I. Thorsos, and D. B. Percival, "Fine-scale volume heterogeneity measurements in sand," *IEEE J. Oceanic Eng.*, vol. 27, pp. 546–560, July 2002.
[9] R. A. Wheatcroft, "*In situ* measurements of near-surface porosity in shallow marine sands," *IEEE J. Oceanic Eng.*, vol. 27, pp. 561–570, July 2002.
[10] R. Ehrlich, S. Kennedy, S. J. Crabtree, and R. L. Cannon, "Petrographic image analysis, I, Analysis of reservoir pore complexes," *J. Sediment. Petrol.*, vol. 54, no. 4, pp. 1365–1378, 1984.
[11] J. Koplik, C. Lin, and M. Vermette, "Conductivity and permeability from microgeometry," *J. Appl. Phys.*, vol. 56, pp. 3127–3131, 1984.
[12] P. M. Doyen, "Permeability, conductivity, and pore geometry of sandstone," *J. Geophys. Res.*, vol. 93, no. B7, pp. 7729–7740, 1988.
[13] J. V. White, B. L. Kirkland, and J. P. Gournay, "Quantitative porosity determination of thin sections using digitized images," *J. Sedim. Res.*, vol. 68, pp. 220–222, 1998.
[14] J. Koplik, "Creeping flow in two-dimensional networks," *J. Fluid Mech.*, vol. 119, pp. 219–247, 1982.
[15] A. E. Scheidegger, *The Physics of Flow Through Porous Media*. New York: MacMillan, 1960.
[16] C. W. Fetter, *Applied Hydrogeology*. New York: Simon and Schuster, 1994.
[17] C. David, "Geometry of flow paths for fluid transport in rocks," *J. Geophys. Res.*, vol. 98 , no. B7, pp. 12 267–12 278, 1993.
[18] P. Carman, *Flow of Gases Through Porous Media*. New York: Academic, 1956.
[19] J. Bear, *Dynamics of Fluids in Porous Media*. New York: Dover, 1972.
[20] M. B. Clennell, "Tortuosity: A guide through the maze," in *Developments in Petrophysics*, M. A. Lovell and P. K. Harvey, Eds. Bath, U.K.: Geological Society Special Publication no. 122, pp. 299–344.
[21] T. J. Plona and D. L. Johnson, "Acoustic properties of porous systems: I Phenomenological description," in *Physics and Chemistry of Porous Media*, D. L. Johnson and P. N. Sen, Eds. New York: American Institute of Physics, 1984, pp. 89–104.
[22] P. D. Jackson, K. B. Briggs, R. C. Flint, R. J. Holyer, and J. C. Sandidge, "Two- and three-dimensional heterogeneity in carbonate sediments using resistivity imaging," *Mar. Geol.*, vol. 182, no. 1/2, pp. 55–76, 2002.
[23] P. D. Jackson, D. Taylor Smith, and P. N. Stanford, "Resistivity-porosity-particle shape relationships for marine sands," *Geophys.*, vol. 43, no. 6, pp. 1250–1268, 1978.
[24] R. H. Bennett, K. M. Fischer, D. L. Lavoie, W. R. Bryant, and R. Rezak, "Porometry and fabric of marine clay and carbonate sediments: Determinants of permeability," *Mar. Geotechnol.*, vol. 89, no. 1/2, pp. 127–152, 1989.
[25] I. Hidajat, A. Rastogi, M. Singh, and K. K. Mohanty, "Transport properties of porous media from thin-sections," in *Proc. SPE' 69 623*, vol. 7.
[26] F. S. Anselmetti, S. Luthi, and G. P. Eberli, "Quantitative characterization of carbonate pore systems by digital image analysis," *AAPG Bull.*, vol. 82, pp. 1815–1836, 1998.
[27] J. G. Berryman and S. C. Blair, "Kozeny–Carman relations and image processing methods for estimating Darcy's constant," *J. Applied Phys.*, vol. 62, no. 6, pp. 2221–2228, 1987.
[28] A. H. Reed, R. B. Pandey, and D. L. Lavoie, "Fractal dimensionality of pore and grain volume of a siliciclastic marine sand," *Inter. J. Mod. Phys. C*, vol. 11, no. 8, pp. 1555–1559, 2000.
[29] T. Bourbie, O. Coussy, and B. Zinszner, *Acoustics of Porous Media*. Houston, TX: Gulf Publishing, pp. 40–42.
[30] V. Clausnitzer and J. W. Hopmans, "Determination of phase-flow fractions from tomographic measurements in two-phase systems," *Adv. Water Resources*, vol. 22, no. 6, pp. 577–584, 1999.
[31] B. Lindquist and W. Oh, "Image thresholding by indicator kriging," *IEEE Trans. Pattern Anal. Machine Intell.*, vol. 21, pp. 919–927, Oct. 1999.
[32] R. Ehrlich, S. J. Crabtree, K. O. Horkowitz, and J. P. Horkowitz, "Petrography and reservoir physics I: Objective classification of reservoir porosity," *J. Sediment. Petrol.*, vol. 75, no. 10, pp. 1547–1562, 1991.
[33] R. Ehrlich, E. L. Etris, D. Brumfield, L. P. Yuan, and S. J. Crabtree, "Petrography and reservoir physics III: Physical models for permeability and formation factor," *Amer. Assoc. Pet. Geol. Bull.*, vol. 75, no. 16, pp. 1579–1592, 1991.
[34] R. W. Mair, G. P. Wang, D. Hoffman, M. D. Hurlimann, S. Patz, L. M. Schwartz, and R. L. Walsworth, "Probing porous media with gas diffusion NMR," *Phys. Rev. Lett.*, vol. 83, pp. 3324–3327, 1999.
[35] C. David, Y. Gueguen, and G. Pampoukis, "Effective medium theory and network theory applied to transport properties of rock," *J. Geophys. Res.*, vol. 95 B5, no. 4, pp. 6993–7005, 1990.
[36] S. Kirkpatrick, "Percolation and conduction," *Rev. Mod. Phys.*, vol. 45, no. 4, pp. 574–588, 1972.
[37] M. Blunt and P. King, "Relative permeabilities from two- and three-dimensional pore-scale network models," *Transport Porous Media*, vol. 6, no. 4, pp. 407–433, 1991.
[38] I. Fatt, "The network model of porous media I. Dynamic properties of networks with tube radius distribution," *Pet. Trans. AIME*, vol. 207, no. 1, pp. 144–159, 1956.
[39] L. J. Doyle and T. N. Sparks, "Sediments of the Mississippi, Alabama and Florida (MAFLA) continental shelf," *J. Sediment. Petrol.*, vol. 50, no. 3, pp. 905–915, 1980.
[40] N. J. Hyne and H. G. Goodell, "Origin of the sediments and submarine geomorphology of the inner continental shelf off Choctawhatchee Bay, Florida," *Mar. Geol.*, vol. 5, pp. 299–313, 1967.
[41] S. D. Locker and L. J. Doyle, "Neogene to Recent stratigraphy and depositional regimes of the northwest Florida inner continental shelf," *Mar. Geol.*, vol. 104, no. 1/4, pp. 123–138, 1992.
[42] D. H. Krinsley and J. C. Doornkamp, *Atlas of Quartz Sand Surface Textures*. Cambridge, U.K.: University Printing House, 1973.
[43] K. B. Briggs, "High-frequency acoustic scattering from sediment interface roughness and volume inhomogeneities," Ph.D. dissertation, Univ. of Miami, Coral Gables, FL, 1994.
[44] R. L. Folk, *Petrology of Sedimentary Rocks*. Austin, TX: Hemphills, 1965.
[45] M. D. Richardson, K. B. Briggs, S. J. Bentley, D. J. Walter, and T. H. Orsi, "The effects of biological and hydrodynamic on physical and acoustic properties of sediments off the Eel River, California," *Mar. Geol.*, vol. 182, no. 1/2, pp. 121–139, 2002.
[46] A. Gaither, "A study of porosity and grain relationships in experimental sands," *J. Sediment. Petrol.*, vol. 23, no. 3, pp. 108–195, 1953.
[47] W. E. Brown and H. W. Patnode, "Plastic lithification of sands *in situ*," *Bull. Amer. Assoc. Petrol. Geol.*, vol. 37, no. 1, pp. 152–162, 1951.
[48] J. H. Schroeder and K. Jacob, "*In situ* impregnation of cores and profiles in coastal sediments," *Senckenberg. marit.*, vol. 8, no. 1, pp. 81–89, 1976.
[49] R. M. McMullen and J. R. L. Allen, "Preservation of sedimentary structures in wet unconsolidated sands using polyester casting resins," *Mar. Geol.*, vol. 1, no. 1, pp. 88–97, 1964.
[50] C. Russ, Reindeer Games, Inc., Gainesville, FL, The Image Processing Toolkit 4.0.
[51] D. C. Wilcox, B. S. Dove, W. D. McDavid, and D. D. Greer, "UTHSCA Image Tool 2.0," University of Texas Health and Science Center, San Antonio, TX, 1989.
[52] M. C. Powers, "A new roundness scale for sedimentary particles," *J. Sediment. Petrol.*, vol. 23, no. 2, pp. 117–119, 1953.
[53] R. H. Bennett, M. H. Hulbert, C. Curry, H. P. Johnson, M. Hutnak, and K. J. Curry, "*In situ* permeameter probe for coastal marine sediments," *IEEE J. Oceanic Eng.*, vol. 27, pp. 571–580, July 2002.
[54] K. B. Briggs, unpublished data.
[55] ASTM Committee D-18, "ASTM D 4253-83: Standard test methods for the maximum index density of soils using a vibratory table," in *Annual Book of ASTM Standards*. W. Conshonocken, PA: ASTM International, 1983, pp. 589–600.
[56] H. J. Frazer, "Experimental study of porosity and permeability of clastic sediments," *J. Geol.*, vol. 43, pp. 910–1010, 1935.

Allen H. Reed received the B.S. degree in oceanography from Humboldt State University, Arcata, CA in 1996, and the M.S. degree in marine sciences from the University of Southern Mississippi, Hattiesburg, in 1999. He is currently working toward the Ph.D. degree in oceanography at the Louisiana State University, Baton Rouge, with funding provided by the Naval Research Laboratory, Stennis Space Center, MS.

His current research is in three-dimensional network modeling of natural marine sands.

He is a member of the American Geophysical Union and the Acoustical Society of America.

Kevin B. Briggs received the B.S. degree in biology from Florida Atlantic University, Boca Raton, in 1975, the M.S. degree in zoology from the University of Georgia, Athens, in 1978, and the Ph.D. degree in marine geology and geophysics from the University of Miami, Rosenstiel School of Marine and Atmospheric Science, Miami, FL, in 1994.

He began working at the Naval Ocean Research and Development Activity, now part of the Naval Research Laboratory (NRL), at the Stennis Space Center in Mississippi in 1979, where he was involved in research on the effects of environmental processes on sediment geoacoustic properties. He has participated in many shallow-water high-frequency acoustics experiments as an investigator of geoacoustic and roughness properties of the seafloor. He is currently engaged in research on characterization of sediment interface roughness and volume heterogeneity for high-frequency acoustic modeling. He has over 30 published articles on physical and acoustic properties of the sea floor.

Dr. Briggs is a member of the Acoustical Society of America, the American Geophysical Union, and Sigma Xi.

Dawn L. Lavoie received the M.S. degree in earth science from the University of New Orleans in 1982, and the Ph.D. degree in Oceanography from Texas A&M University, College Station, in 1988.

She was a Marine Geologist/Oceanographer with the Naval Ocean Research and Development Activity and Naval Research Laboratory, Stennis Space Center, MS, for 19 years, where she performed research on physical and geotechnical properties of marine sediments. She served as Program Officer for Marine Geosciences and the Mine Burial Program at the Office of Naval Research, Arlington, VA, during 2001-2002. She is presently Associate Director for Coastal and Marine Geology at the U.S. Geological Survey, (USGS), Arlington, VA.